

Article

Dihydroconiferyl Ferulate Isolated from *Dendropanax morbiferus* H.Lév. Suppresses Stemness of Breast Cancer Cells via Nuclear EGFR/c-Myc Signaling

Yu-Chan Ko ^{1,†}, Ren Liu ^{1,†}, Hu-Nan Sun ² , Bong-Sik Yun ³, Hack Sun Choi ^{4,5,*} and Dong-Sun Lee ^{1,4,5,6,*} 

- ¹ Interdisciplinary Graduate Program in Advanced Convergence Technology and Science, Jeju National University, Jeju 63243, Korea; uchan@jejunu.ac.kr (Y.-C.K.); liuren0308@gmail.com (R.L.)
- ² Stem Cell Therapy and Regenerative Biology Laboratory, College of Life Science and Biotechnology, Heilongjiang Bayi Agricultural University, Daqing 163319, China; sunhunan76@163.com
- ³ Division of Biotechnology, College of Environmental and Bioresource Sciences, Jeonbuk National University, Gobong-ro 79, Iksan 54596, Korea; bsyun@jbnu.ac.kr
- ⁴ Subtropical/Tropical Organism Gene Bank, Jeju National University, Jeju 63243, Korea
- ⁵ Jeju Microbiome Research Center, Jeju National University, Jeju 63243, Korea
- ⁶ Faculty of Biotechnology, College of Applied Life Sciences, SARI, Jeju National University, Jeju 63243, Korea
- * Correspondence: choix074@jejunu.ac.kr (H.S.C.); dongsunlee@jejunu.ac.kr (D.-S.L.)
- † These authors contributed equally to this work.

Abstract: Breast cancer is the leading cause of global cancer incidence and breast cancer stem cells (BCSCs) have been identified as the target to overcome breast cancer in patients. In this study, we purified a BCSC inhibitor from *Dendropanax morbiferus* H.Lév. leaves through several open column and high-performance liquid chromatography via activity-based purification. The purified cancer stem cell (CSC) inhibitor was identified as dihydroconiferyl ferulate using nuclear magnetic resonance and mass spectrometry. Dihydroconiferyl ferulate inhibited the proliferation and mammosphere formation of breast cancer cells and reduced the population of CD44^{high}/CD24^{low} cells. Dihydroconiferyl ferulate also induced apoptosis, inhibited the growth of mammospheres and reduced the level of total and nuclear EGFR protein. It suppressed the EGFR levels, the interaction of Stat3 with EGFR, and c-Myc protein levels. Our findings show that dihydroconiferyl ferulate reduced the level of nuclear epidermal growth factor receptor (EGFR) and induced apoptosis of BCSCs through nEGFR/Stat3-dependent c-Myc deregulation. Dihydroconiferyl ferulate exhibits potential as an anti-CSC agent through nEGFR/Stat3/c-Myc signaling.

Keywords: breast cancer stem cells; dihydroconiferyl ferulate; nuclear EGFR; Stat3; c-Myc



Citation: Ko, Y.-C.; Liu, R.; Sun, H.-N.; Yun, B.-S.; Choi, H.S.; Lee, D.-S. Dihydroconiferyl Ferulate Isolated from *Dendropanax morbiferus* H.Lév. Suppresses Stemness of Breast Cancer Cells via Nuclear EGFR/c-Myc Signaling. *Pharmaceuticals* **2022**, *15*, 664. <https://doi.org/10.3390/ph15060664>

Academic Editors: Víctor López and Filippo Maggi

Received: 6 April 2022

Accepted: 22 May 2022

Published: 26 May 2022

Publisher's Note: MDPI stays neutral with regard to jurisdictional claims in published maps and institutional affiliations.



Copyright: © 2022 by the authors. Licensee MDPI, Basel, Switzerland. This article is an open access article distributed under the terms and conditions of the Creative Commons Attribution (CC BY) license (<https://creativecommons.org/licenses/by/4.0/>).

1. Introduction

Breast cancer develops from breast tissue and is ranked fifth in mortality for cancers globally (6.9% of total cancer-related deaths) [1]. In women, breast cancer is the most commonly diagnosed and the leading cause of cancer-related deaths [1]. Breast cancer expresses well-characterized immunohistochemical markers (ER, PR, and HER2), proliferation markers (Ki-67), genomic markers (BRCA1, BRCA2, and PIK3CA), and immunologic markers (tumor-infiltrating lymphocytes) [2]. It is a very heterogeneous disease and may be divided into several major subcategories, including hormone-receptor (HR)-positive (HR+; ER+, PR+/-, and HER2-), HER2-positive (HER2+), and triple-negative (TN; ER-, PR-, and HER2-) breast cancer [3]. Compared with patients with other subtypes, TN breast cancer (TNBC) patients exhibit chemoresistance, recurrence, and metastasis [4]. Chemoresistance of breast cancer is associated with the presence of stem-like cells (cancer stem cells (CSCs)) [5]. Breast cancer stem cells (BCSCs) exhibit a capacity for self-renewal and are capable of initiating tumor growth. BCSC markers are designated as CD44^{high}/CD24^{low} [6]. Several signaling pathways and transcription factors of breast CSCs are over-activated,

compared with normal breast cancer cells. For example, the Wnt/ β -catenin pathway is associated with cancer development and is believed to play an important role in the pathogenesis of hepatoblastoma, stem cell self-renewal, and CSC formation [7,8]. Notch signaling plays an important role in the maintenance of stemness of breast cancer cells [9]. The knockdown of tafazzin (TAZ, Hippo pathway) inhibits the self-renewal of BCSCs [10]. Targeting Stat pathways using sulforaphane inhibits endocrine-resistant, stem-like cells in breast cancer [11]. Myc inhibition depletes cancer stem-like cells in triple-negative breast cancer [12]. Interleukin 6 (IL-6) increases the invasive ability, metastatic potential, and stem-like phenotype of breast cancer cells [13]. Interleukin 8 (IL-8) is upregulated in breast cancer and is associated with a high risk of developing large, high-grade tumors [14].

The epidermal growth factor receptor (EGFR) is a membrane-bound receptor tyrosine kinase. It is a member of the ErbB family, which includes EGFR/ErbB-1/HER-1, ErbB-2/HER-2/neu, ErbB-3/HER-3, and ErbB-4/HER-4. ErbB-3 is the only member that does not exhibit tyrosine kinase activity [15]. EGFR is involved in multiple signaling pathways, including the PI3K/AKT, RAS/Raf/MAPK, JNK/STAT, and PLC γ /PKC pathways, which are associated with cell proliferation, DNA replication, and poor clinical outcomes [16–19]. Over the last few decades, many studies have demonstrated EGFR overexpression in TNBCs and its internalization from the cell membrane to the nucleus [20–22]. The translocated nuclear EGFR (nEGFR), which occurs through clathrin-coated pit-mediated receptor internalization, functions as a transcription factor to regulate the properties of CSCs through nuclear EGFR–PKM2 complexes [23,24]. These studies suggest that targeting nEGFR signaling is important for treating TNBC-derived stem cells.

Dendropanax morbiferus H.Lév. is a flowering plant from the family of *Araliaceae* and is known as a traditional medicinal plant in Korea, China and South America. The leaves, bark, roots, and stems of *Dendropanax morbiferus* H.Lév. are known as a traditional medicine for the prevention of several disorders [25]. The edible parts of *Dendropanax morbiferus* H.Lév. have been used as food additives [25]. The active compounds derived from the *Dendropanax* genus exhibit a broad range of therapeutic applications, including antioxidant, antibacterial, cytotoxic, anti-inflammatory, neuroprotective, antidiabetic, and anticancer properties [25–29]. Because *Dendropanax morbiferus* H.Lév. has pharmacological activities and is beneficial to human health, we isolated an inhibitor against breast CSCs from *Dendropanax morbiferus* H.Lév. on the basis of a mammosphere formation-guided assay. The isolated compound was identified as dihydroconiferyl ferulate, and it inhibits the formation of breast cancer mammospheres. In the present study, the isolated compound was identified as dihydroconiferyl ferulate, which suppresses mammosphere formation in breast cancer cell lines. This study also investigated whether dihydroconiferyl ferulate inhibited breast CSC formation through the EGFR/Stat3/c-Myc signaling pathway.

2. Results

2.1. Dihydroconiferyl Ferulate Isolated from *Dendropanax morbiferus* H.Lév. Suppresses the Mammosphere Formation Rate of Breast Cancer Cells

We purified a breast CSC inhibitor from *Dendropanax morbiferus* H.Lév. via fractionation guided with a mammosphere formation assay of MDA-MB-231 cells. Figure 1A shows the purification procedure. The extracted samples were purified using organic solvent extraction (methanol extraction and ethyl acetate extraction), silica gel, Sephadex LH-20 gel, preparatory TLC, and preparatory HPLC. The isolated compound suppressed the tumorsphere formation of MDA-MB-231 cells (Figure 1B). HPLC data indicated a high purity of the isolated compound (Figure 1C), which was identified as dihydroconiferyl ferulate using NMR and mass data (Figures 2 and S1–S7).

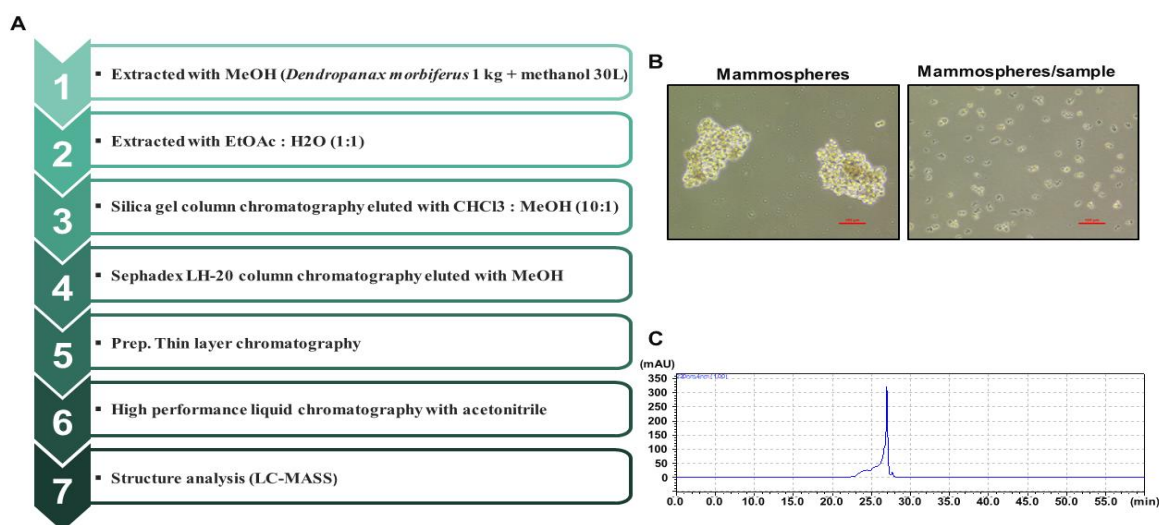
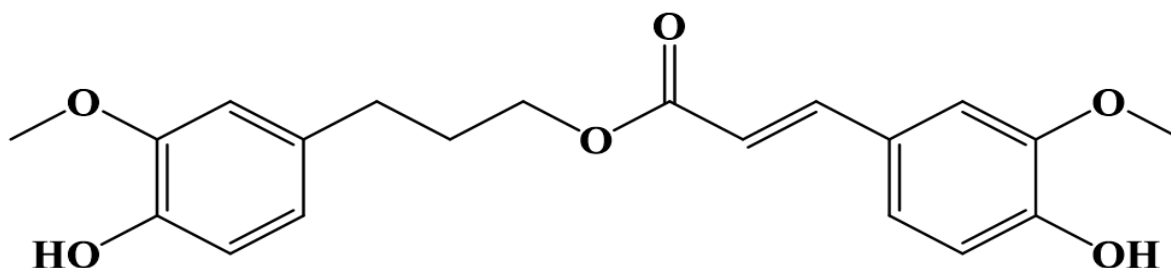


Figure 1. Purification of a breast CSC inhibitor from *Dendropanax morbiferus* H.Lév. using fractionation guided by a mammosphere assay. (A) Isolation protocol for the inhibitor of mammosphere formation from *Dendropanax morbiferus* H.Lév. (B) Effect of the purified inhibitor from *Dendropanax morbiferus* H.Lév. on mammosphere formation using MDA-MB-231 cells. Images were analyzed using microscopy at 10× magnification (scale bar = 100 μm). (C) HPLC data for the isolated samples from *Dendropanax morbiferus* H.Lév.



Dihydroconiferyl ferulate (MW: 358)

Figure 2. Molecular structure of the cancer stem cell inhibitor from *Dendropanax morbiferus* H.Lév.

To determine whether dihydroconiferyl ferulate has a potent inhibitory effect on human breast cancer cells, we first tested the anti-proliferative effect on dihydroconiferyl ferulate at various concentrations in MCF-7 and MDA-MB-231 cells. Dihydroconiferyl ferulate inhibited the proliferation of MDA-MB-231 (Figure 3A) and MCF-7 (Figure 3B) cells at 75 μM. The IC₅₀ value (the drug concentration required for 50% growth reduction in the survival curve) of MCF-7 and MDA-MB-231 cells was 112.4 μM and 114.6 μM, (Figure 3A,B) respectively. The results indicated that dihydroconiferyl ferulate suppresses breast cancer cell proliferation.

To find the dihydroconiferyl ferulate inhibitor that possesses a CSC-suppressing effect, we carried out a mammosphere formation assay by automatic counting using the NICE program. To determine whether dihydroconiferyl ferulate can inhibit mammosphere formation, we treated the mammospheres with dihydroconiferyl ferulate. As shown in Figure 3C,D, dihydroconiferyl ferulate decreased the sphere size and number of tumourspheres derived from MDA-MB-231 and MCF-7 cells (Figure 3C,D). The results indicated that dihydroconiferyl ferulate suppresses mammosphere formation.

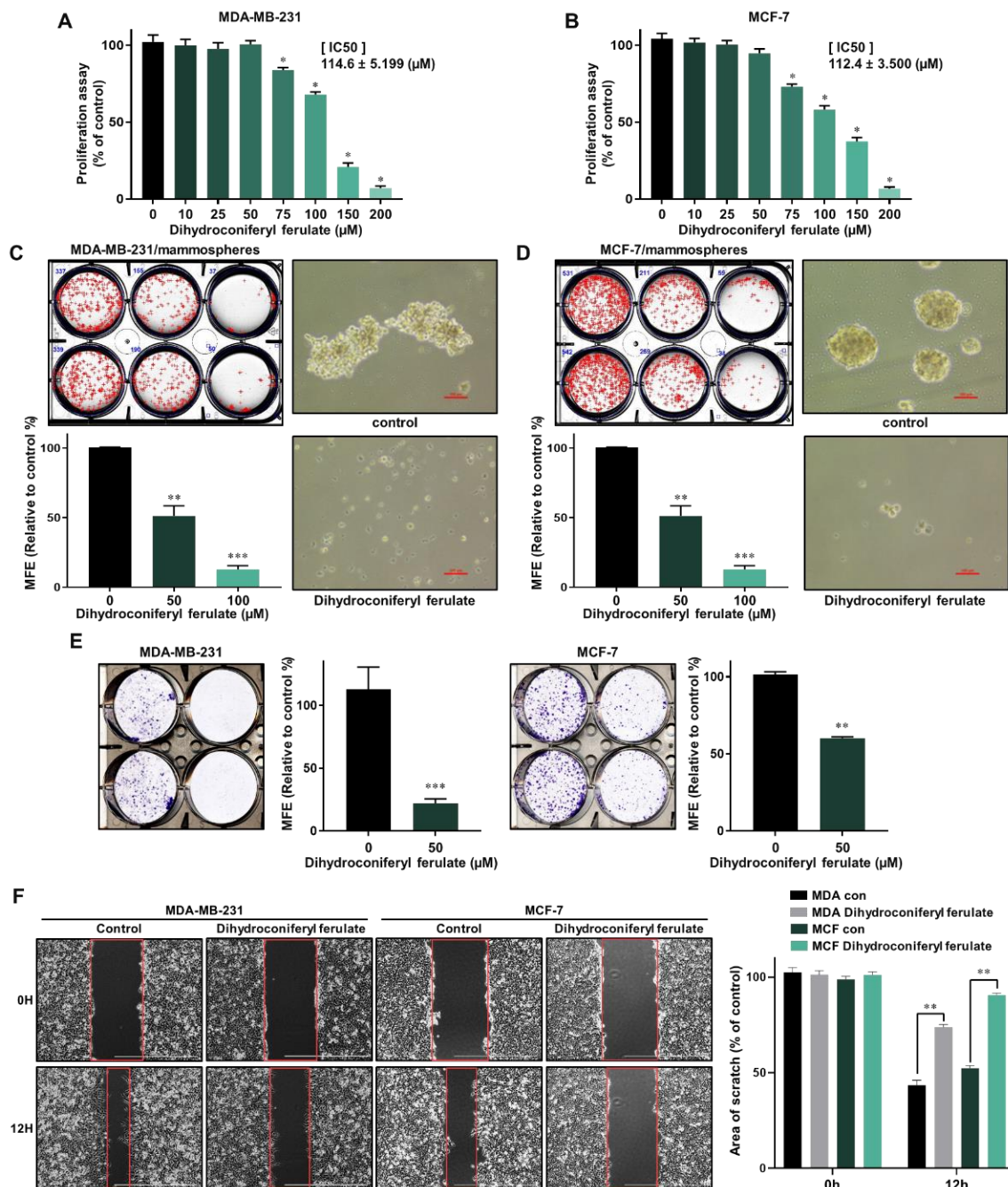


Figure 3. Inhibitory effects of dihydroconiferyl ferulate on cancer cell proliferation and formation of mammospheres. (A,B) The antiproliferative ability of dihydroconiferyl ferulate was determined using a proliferation assay kit with MDA-MB-231 and MCF-7 cells treated with dihydroconiferyl ferulate. * IC_{50} value is the drug concentration required for 50% growth reduction in the survival curve. (C,D) To measure the effect of dihydroconiferyl ferulate on the formation of mammospheres derived from breast cancer cells, they were cultured with increasing concentrations of dihydroconiferyl ferulate. After 7 days, the mammosphere morphologies were analyzed. Representative tumor-sphere images were examined via inverted microscopy at $10\times$ magnification (scale bar = $100 \mu\text{m}$). (E,F) Effects of dihydroconiferyl ferulate on colony formation and migration of breast cancer cells. MDA-MB-231 and MCF-7 cells (1×10^3 per well) were cultured with or without dihydroconiferyl ferulate for 7 days. The colonies were scanned using a scanner. Migration images for dihydroconiferyl ferulate were captured at 12 h (scale bar: $1000 \mu\text{m}$). The percent inhibition of cancer cell migration was determined relative to the untreated control, which was designated 100. Representative data were collected and represent the mean \pm standard deviation; ** $p < 0.01$, *** $p < 0.001$ vs. control.

Since cell colony formation and cell migration are likely to be two important processes in breast cancer tumorigenesis and metastasis, the colony formation and wound-healing assays were performed. As shown in Figure 3E,F, 50 μM of dihydroconiferyl ferulate inhibited colony formation and migration of MDA-MB-231 and MCF-7 cells. Curcumin and dihydroconiferyl ferulate have similar effects on migration and colony formation of breast cancer. The results indicate that dihydroconiferyl ferulate is a strong suppressor of breast cancer cell migration and colony formation.

2.2. Dihydroconiferyl Ferulate Suppresses $\text{CD44}^{\text{high}}/\text{CD24}^{\text{low}}$ Expressing Cells and Mammosphere Growth and Induces Mammosphere Apoptosis

The $\text{CD44}^{\text{high}}/\text{CD24}^{\text{low}}$ subpopulations are breast CSC populations and are a representative marker of breast CSCs. We cultured MDA-MB-231 cells in 6-well culture plates and then treated them with/without dihydroconiferyl ferulate for 24 h and determined the $\text{CD44}^{\text{high}}/\text{CD24}^{\text{low}}$ population in MDA-MB-231 breast cancer cells. Dihydroconiferyl ferulate decreased the $\text{CD44}^{\text{high}}/\text{CD24}^{\text{low}}$ population of breast cancer cells from 80.8% to 34.0% (Figure 4A).

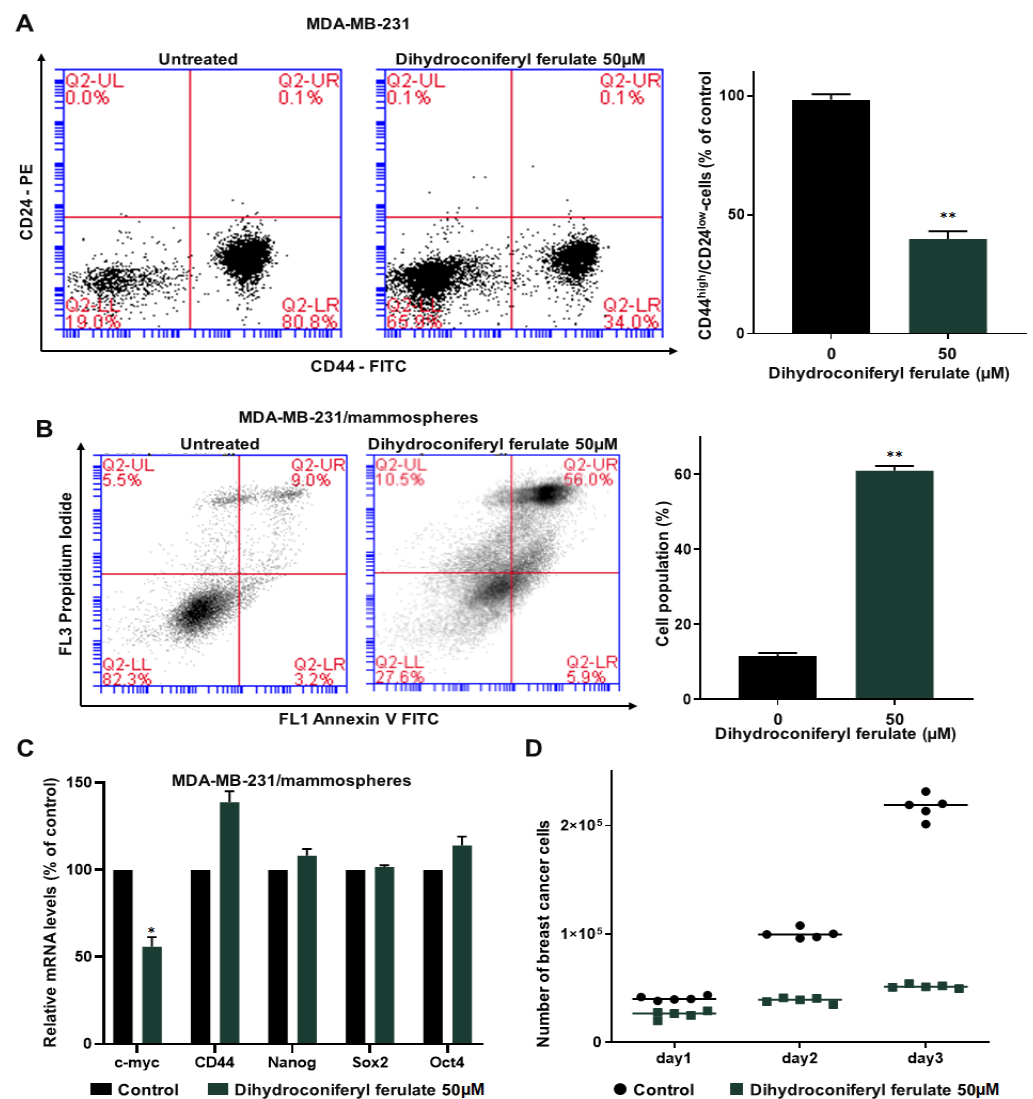


Figure 4. Dihydroconiferyl ferulate suppresses the subpopulations of $\text{CD44}^{\text{high}}/\text{CD24}^{\text{low}}$ and the growth of mammospheres and induces apoptosis of mammospheres. (A) MDA-MB-231 cells were

treated with dihydroconiferyl ferulate (50 μM) for 24 h. The CD44^{high}/CD24^{low} populations of breast cancer cells were examined by flow cytometry. (B) MDA-MB-231 tumorspheres were cultured for 5 days and then treated with dihydroconiferyl ferulate (50 μM) for 48 h. Tumorspheres were segregated into single cells and apoptosis was measured with an Annexin V/PI assay kit. (C) Transcripts for the CSC markers, Oct4, CD44, Sox2, c-myc, and Nanog, were examined in mammospheres treated with dihydroconiferyl ferulate using gene-specific primers by qRT-PCR (Table S1). β -actin was used as a control. (D) Dihydroconiferyl ferulate suppresses mammosphere growth. Mammospheres treated with dihydroconiferyl ferulate were segregated into single cells and an equal number of cells were seeded into 6 cm culture dishes. The cells were counted at 24, 48, and 72 h. Representative data were collected and represent the mean \pm standard deviation; * $p < 0.05$, ** $p < 0.01$ vs. control.

To determine whether dihydroconiferyl ferulate induces apoptosis of breast CSCs and inhibits mammosphere growth, 5 day cultured mammospheres were treated with or without dihydroconiferyl ferulate (50 μM). The results indicated that dihydroconiferyl ferulate induced breast CSC apoptosis (Figure 4B).

To examine whether dihydroconiferyl ferulate regulates CSC-specific gene expression, we examined the transcription of CSC-specific genes using RT-qPCR. The dihydroconiferyl ferulate decreased c-Myc gene expression (Figure 4C). To confirm that dihydroconiferyl ferulate inhibits the proliferation of mammospheres, we incubated dihydroconiferyl ferulate on mammospheres and counted the cell numbers. Dihydroconiferyl ferulate reduced the cell number of dihydroconiferyl ferulate-incubated mammospheres and killed cells of mammospheres. These data indicated that dihydroconiferyl ferulate leads to a dramatic reduction in mammosphere growth (Figure 4D).

2.3. Dihydroconiferyl Ferulate Reduces the Total and Nuclear Levels of EGFR in Breast CSCs

To identify the underlying molecular mechanism associated with the inhibition of mammosphere formation by dihydroconiferyl ferulate, we measured the total and nuclear levels of EGFR via Western blot analysis. The total and nuclear levels of EGFR protein were significantly reduced after a 48 h treatment with dihydroconiferyl ferulate (50 μM) (Figure 5A,B).

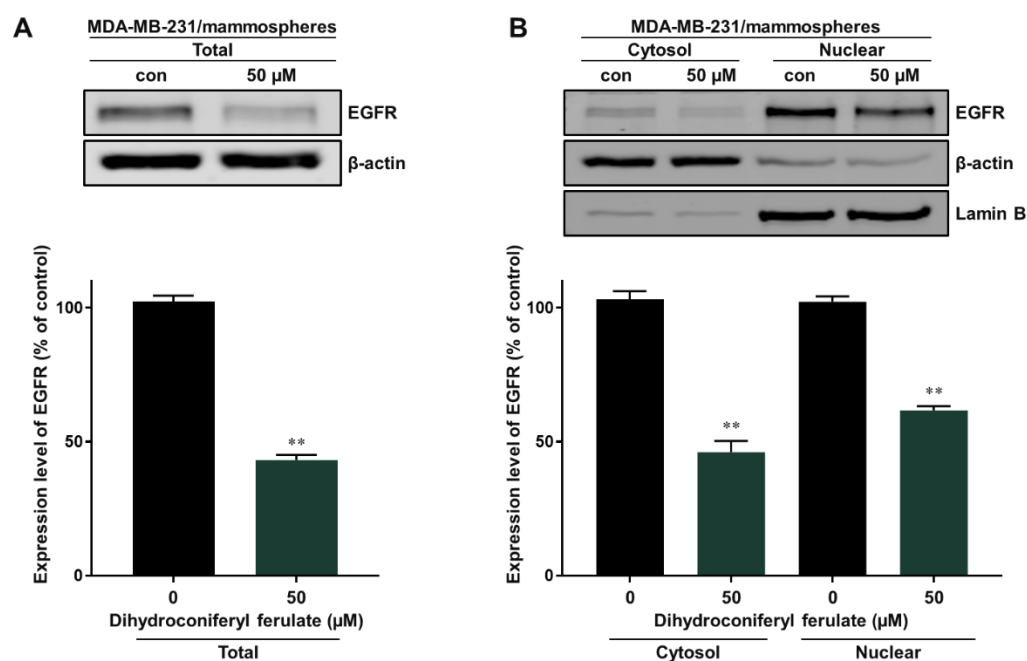


Figure 5. Inhibitory effect of dihydroconiferyl ferulate on EGFR signaling. (A) Western blot analysis showing the level of total EGFR measured in tumorspheres derived from MDA-MB-231 cells after

treatment with dihydroconiferyl ferulate (50 μM) or DMSO for 48 h. (B) The nuclear protein levels of EGFR were examined in MDA-MB-231-derived mammospheres treated with dihydroconiferyl ferulate (50 μM). Dihydroconiferyl ferulate decreases the total and nuclear protein levels of EGFR. Data from the experiments represent the mean \pm standard deviation; ** $p < 0.01$ vs. control.

2.4. Dihydroconiferyl Ferulate Inhibits the Interaction of EGFR with Stat3 and Decreases the Total and Nuclear Levels of pStat3 and Stat3 in Breast CSCs

Breast cancer cells overexpress the EGFR protein and EGFR exhibits membrane-bound and nuclear signaling activities. Nuclear EGFR induces resistance to anti-EGFR therapy and is a therapeutic target for breast cancer. Nuclear EGFR (nEGFR) is also a regulator and cofactor of Stat3 [30–33]. We evaluated the interaction between Stat3 and EGFR protein using immunoprecipitation. Dihydroconiferyl ferulate inhibited the interaction of EGFR and Stat3 (Figure 6A). Subsequently, the total and nuclear levels of p-Stat3 and Stat3 protein were assessed using Western blot analysis. Dihydroconiferyl ferulate decreased the total level of p-Stat3 (Figure 6B), as well as cytosolic and nuclear p-Stat3 and Stat3 levels (Figure 6C).

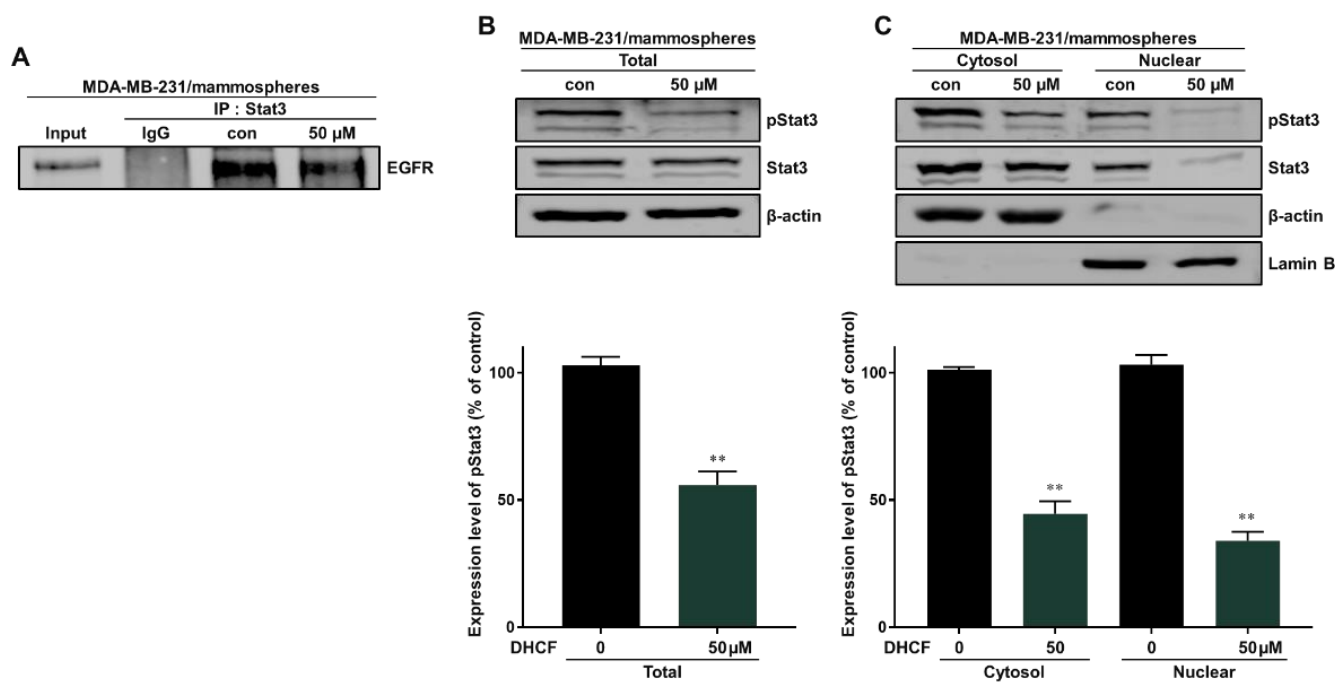


Figure 6. Dihydroconiferyl ferulate inhibits the interaction between EGFR and Stat3. (A) Stat3 and EGFR were immunoprecipitated with anti-Stat3 antibody from mammosphere extracts after treatment with dihydroconiferyl ferulate (50 μM) for 48 h. Immunoblotting was carried out using the anti-EGFR antibody. (B) Results of immunoblot analysis showing the levels of pStat3 and Stat3 in total proteins measured in mammosphere extracts after treatment with dihydroconiferyl ferulate (50 μM) for 48 h. (C) The nuclear levels of pStat3 and Stat3 proteins were determined in mammospheres derived from MDA-MB-231 treated with dihydroconiferyl ferulate (50 μM) or DMSO for 48 h. Dihydroconiferyl ferulate decreased the levels of p-Stat3 and Stat3 in mammospheres. Data from experiments represent the mean \pm standard deviation; ** $p < 0.01$ vs. control.

2.5. Dihydroconiferyl Ferulate Decreases the Transcript Level of c-Myc and Inhibits the Total and Nuclear Levels of c-Myc Protein

Nuclear EGFR is known to function as a co-transcription factor of Stat3 to enhance the transcription of the c-myc gene [30]. We examined the inhibitory effect on c-Myc transcription through the EGFR-Stat3 complex, which was inhibited by dihydroconiferyl ferulate treatment. The relative mRNA and protein expression of c-Myc were determined following dihydroconiferyl ferulate (50 μM) exposure. As shown in Figure 7A,B, dihydro-

coniferyl ferulate decreased c-Myc mRNA levels, as well as the total and nuclear levels of c-Myc protein (Figure 7C,D). The downregulation of Stat3 also decreased the protein and mRNA expression levels of c-Myc (Figure 7E,F). Additionally, c-Myc knockdown inhibited mammosphere formation (Figure 7G). This suggests that dihydroconiferyl ferulate inhibits c-Myc expression via Stat3 and/or EGFR-Stat3 complex inhibition. Figure 8 shows a schematic illustration of the proposed mechanism through which dihydroconiferyl ferulate inhibits breast CSC formation via the EGFR-Stat3/c-Myc signaling pathway.

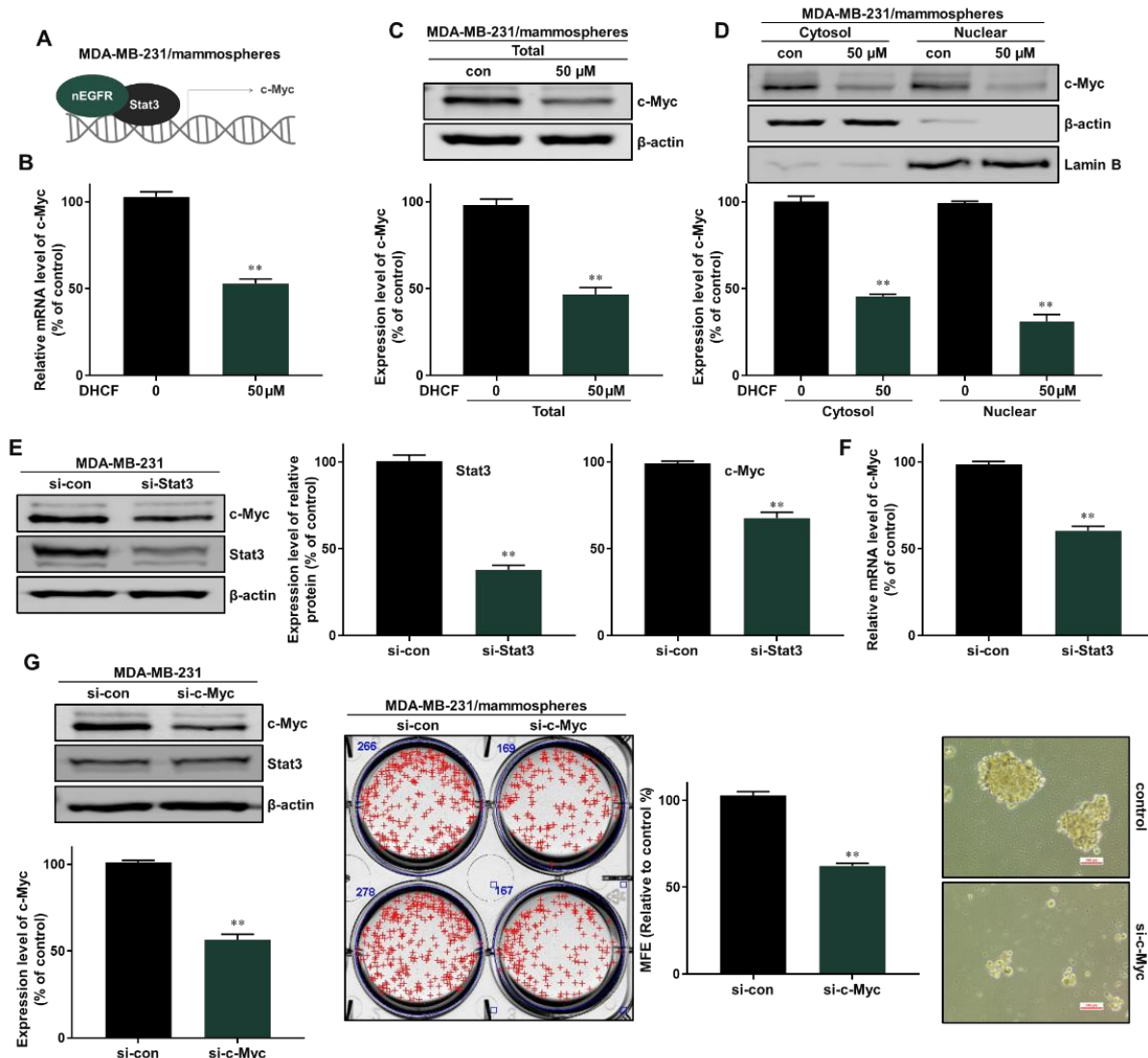


Figure 7. Dihydroconiferyl ferulate inhibits the c-Myc pathway via Stat3/nEGFR. (A,B) The relative mRNA levels of c-Myc were measured in mammospheres after treatment with dihydroconiferyl ferulate (50 μM) for 48 h. Dihydroconiferyl ferulate reduces the mRNA levels of c-Myc. (C) The expression level of c-Myc in total protein from MDA-MB-231 mammospheres treated with dihydroconiferyl ferulate (50 μM) for 48 h. Dihydroconiferyl ferulate reduces the expression of c-Myc. (D) The nuclear protein level of c-Myc was determined in mammospheres derived from MDA-MB-231 cells treated with dihydroconiferyl ferulate (50 μM) for 48 h. Dihydroconiferyl ferulate decreases the level of c-Myc in mammospheres. (E) The protein levels of Stat3 and c-Myc in MDA-MB-231 cells treated with a specific Stat3 siRNA. Knockdown of Stat3 decreased the expression of c-Myc. (F) qRT-PCR analysis of c-Myc in MDA-MB-231 cells treated with a specific Stat3 siRNA. (G) The protein levels of Stat3 and c-Myc in MDA-MB-231 cells treated with a specific c-Myc siRNA. Knockdown of c-Myc does not affect the expression of Stat3. Knockdown of c-Myc inhibits mammosphere formation. Representative data were collected and the data represent the mean ± standard deviation; ** $p < 0.01$ vs. control.

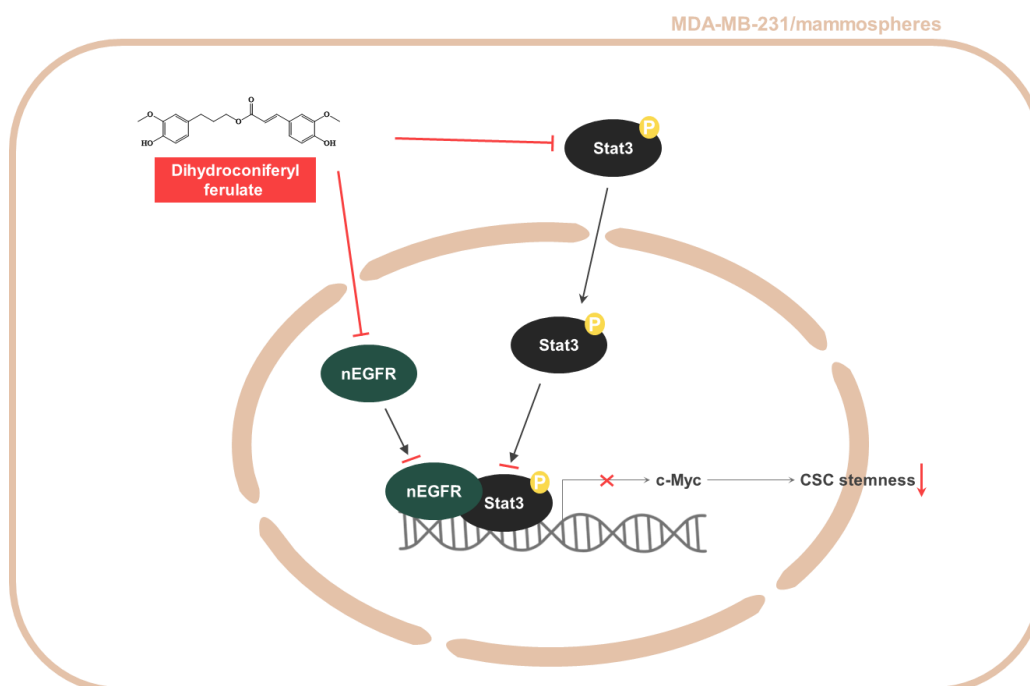


Figure 8. Schematic summary of breast CSC formation via the Stat3/nEGFR/c-Myc signaling pathway induced by dihydroconiferyl ferulate.

3. Discussion

Dendropanax morbiferus H.Lév. is a traditional medicinal plant that belongs to Araliaceae. Previous studies have shown that *Dendropanax morbiferus* H.Lév. exerts various biological activities, including antifungal [34], antibacterial [34], cytotoxic [35,36], antidiabetic [37], antioxidant [38,39], anti-inflammatory [40,41], hepatoprotective [42], neuroprotective [43,44], and anticancer [45] activities. The bioactive compounds contained in *Dendropanax morbiferus* H.Lév. have been summarized by R.B. et al. [25] and include flavonoids, pyrimidines, terpenoids, polyphenols, tannins, essential oils, alkaloids, and phenol carboxylic acids, such as lutein, β -sitosterol, chlorogenic acid, protocatechuic acid, quercetin, trans-ferulic acid, caffeic acid, and resveratrol. The extract of *Dendropanax morbifera* Léveille caused an increase in apoptotic or senescent cells in Huh-7 cells and caused the activation of p16 and p53 pathways. The inhibition of Akt or ERK signaling resulted in the suppression of Huh-7 cell proliferation [26].

In the present study, we isolated a compound from *Dendropanax morbiferus* H.Lév. via multiple chromatography steps using activity-guided fractionation (Figures 1 and S8–S12). The resulting compound was identified as dihydroconiferyl ferulate via ESI-MS and NMR (Figures 2 and S1–S7). Subsequently, the inhibitory effect of dihydroconiferyl ferulate on breast cancer cell proliferation and mammosphere formation was demonstrated. As shown in Figure 3, dihydroconiferyl ferulate inhibits the proliferation of TNBC, MDA-MB-231, and ER+ MCF-7 cells, as well as mammosphere formation. The expression of the CD44^{high}/CD24^{low} CSC phenotype and the effect of dihydroconiferyl ferulate on stemness in MDA-MB-231 cells was assessed. The results indicated that dihydroconiferyl ferulate decreases the CD44^{high}/CD24^{low} subpopulation from 80.8% to 34% (Figure 4A). The apoptosis and growth of breast CSCs were determined following dihydroconiferyl ferulate (50 μ M) treatment. As shown in Figure 4B,D, dihydroconiferyl ferulate inhibited breast cancer stem cell growth and induced apoptosis. The structure of dihydroconiferyl ferulate is similar to that of butein and curcumin. Butein is an active flavonoid isolated from the bark of *Rhus verniciflua* and exhibits anticancer activity against various human cancer cell types, including osteosarcoma, colon carcinoma, breast carcinoma, hepatocarcinoma, and lymphoma [46–50]. Previous studies have shown that butein induces an apoptotic effect

in hepatic cells by decreasing Stat3-related gene expression [51]. Butein also suppresses the protein tyrosine kinase activity of EGFR in HepG2 cells [52] and circumvents gefitinib-resistant lung cancer growth by inhibiting EGFR [53]. Curcumin is a polyphenol compound that is isolated from *Curcuma longa* and exhibits therapeutic benefits in various types of cancers. The primary molecular targets of curcumin are Stat3, Stat5, Notch-1, NF- κ B, VEGF, and interleukins [54]. Curcumin potentiates the anticancer activity of gefitinib both in vitro and in vivo through the inhibition of EGFR phosphorylation and induces EGFR ubiquitination in non-small cell lung cancer [55]. EGFR is also a co-transcription factor that regulates c-fos, cyclin D1, inducible nitric oxide synthase (iNOS), cyclooxygenase-2 (COX-2), and aurora kinase A [31,56–58]. EGFR regulates stemness in several cancer types and treatment of EGFR inhibitors regulates the appearance of stemness in lung cancer cells [59].

Using these data, we determined the level of total and nuclear EGFR protein in mammospheres following dihydroconiferyl ferulate treatment. The results indicated that dihydroconiferyl ferulate decreases the expression of both total and nuclear EGFR (Figure 5). Nuclear EGFR interacts with Stat3 to form a complex, which can regulate the expression of IL-6 and c-Myc [32]. Dihydroconiferyl ferulate inhibited the nEGFR/Stat3 complex (Figure 6A) and decreased the phosphorylation of Stat3 in total lysates prepared from mammospheres (Figure 6B). Moreover, dihydroconiferyl ferulate decreased the nuclear levels of pStat3 and Stat3 protein (Figure 6C). The inhibition of the nEGFR/Stat3 complex resulted in the downregulation of c-Myc transcription following dihydroconiferyl ferulate treatment (Figure 7A,B) and reduced the total and nuclear levels of c-Myc (Figure 7C,D). The knockdown of Stat3 using si-RNA inhibited the transcription and expression of c-Myc (Figure 7E,F), whereas the knockdown of c-Myc resulted in the inhibition of mammosphere formation (Figure 7G). *Dendropanax morbifera* extracts have anti-cancer effects on MCF-7 and MDA-MB-231 cells. However, our isolated and analyzed compound has anti-CSC effects. We also confirmed the mechanism of how this compound inhibits breast cancer stem cells. Our results showed that dihydroconiferyl ferulate has potential as an anti-CSC agent. Dihydroconiferyl ferulate inhibited the growth of breast cancer cells and mammospheres. Cell colony formation and cell migration are likely to be two important processes in breast cancer tumorigenesis and metastasis. Metastasis is known to cause high rates of recurrence and mortality in cancer patients. Our inhibitor suppressed the migration and colony formation of the breast cancer cells (Figure 3). In the present study, the isolated compound, dihydroconiferyl ferulate, suppresses mammosphere formation in breast cancer cell lines. Our data showed that dihydroconiferyl ferulate inhibited breast CSC formation through the EGFR/Stat3/c-Myc signaling pathway. Our data suggest that dihydroconiferyl ferulate provides a new compound for breast cancer therapy by targeting EGFR signaling.

4. Materials and Methods

4.1. Chemicals and Reagents

Silica gel 60 powder and silica gel 60 F₂₅₄ aluminum sheets and glass plates for thin-layer chromatography (TLC) were obtained from Merck Supelco (Darmstadt, Hesse, Germany). Sephadex LH-20 (LH20_100) powder was obtained from Millipore (Cytiva, Marlborough, MA, USA). High-pressure liquid chromatography (HPLC) was conducted using a Shimadzu LC-10 system (Tokyo, Japan). Breast cancer cell viability was determined using a cell viability assay kit (EZ-Cytox, DoGenBio, Seoul, Korea). The other chemicals and organic solvents were obtained from Sigma (St. Louis, MO, USA).

4.2. Plant Material Source

Dried *Dendropanax morbiferus* H.Lév. leaves were obtained from urban farmers (Seogwipo, Jeju, Korea). The *Dendropanax morbiferus* H.Lév. leaves were ground. A sample (no. 2020_011) was deposited at the Faculty of Biotechnology, Jeju National University (Jeju-Si, Korea). The authenticator of the plant material, such as the leaves of the *Dendropanax morbiferus* plant identified by Professor Yong-Suk Chung (Jeju National University).

4.3. Isolation of an Inhibitor of Mammosphere Formation from *Dendropanax morbiferus* H.Lév.

For organic solvent extraction, the method for the isolation of a mammosphere formation inhibitor from *Dendropanax morbiferus* H.Lév. was described previously [60]. *Dendropanax morbiferus* H.Lév. powder (1000 g) was added to methanol and the mixture was extracted (MeOH 30 L). Figure 1A summarizes the isolation procedure. *Dendropanax morbiferus* H.Lév. (40 g) powder was extracted with 1.2 L of methanol in a 3 L flask (total 25 flasks) at 30 °C overnight, using a shaking incubator. The methanol extracts were filtered with filter paper (ADVANTEC®, Niigata, Japan) and evaporated from 30 L to 5 L for 10 h using a rotary evaporator (Heidolph, Schwabach, Germany). It was mixed with a 2-fold volume of water ($v/v = 1:2$), and the methanol was evaporated from the mixture at 55 °C. The water-suspended mixture was extracted with an equal volume of ethyl acetate (EA, $v/v = 1:1$) using a separatory funnel (Sigma-Aldrich, Burlington, MA, USA). The ethyl acetate was evaporated at 55 °C using a rotary evaporator for 30 min and then the extracts were dissolved with 200 mL of methanol.

For chromatography, the 10 mL of EA extract was evaporated at 55 °C and then concentrated with 5 mL of chloroform-methanol solvent (CHCl_3 : MeOH, 10:1). It was separated on a silica gel column (3×35 cm; particle size: 40–63 μm), and eluted with a chloroform-methanol solvent (CHCl_3 : MeOH, 10:1, Figure S8). We separated the samples about 20 times. The column was fractionated into six parts on the basis of color. The fractionated samples were evaporated at 55 °C and dissolved with methanol. Then, each fraction was subjected to a mammosphere formation assay. Fraction #4 strongly inhibited mammosphere formation and was further separated into four parts using a Sephadex LH-20 gel column (2.5×30 cm, particle size: 25–100 μm) with methanol (Figure S9). These four fractions were isolated and evaluated using the mammosphere formation assay. Fraction #3 exhibited significant inhibitory activity in the assay; thus, it was loaded onto a preparatory TLC silica gel glass plate (20×20 cm, Merck KGaA, Darmstadt, Germany) and developed in a glass chamber (CHCl_3 : MeOH, 10:1). The major band was scraped out with knife, dissolved with methanol, centrifuged for 5 min, and then concentrated with methanol. Its activity was examined using the mammosphere formation assay (Figure S10).

For HPLC, the active band was analyzed on a HPLC instrument (Shimadzu LC-20A, Kyoto, Japan) with an ODS column (10×250 mm, flow rate: 2 mL/min, mobile phase: acetonitrile-water). The acetonitrile concentration was initiated at 0%, increased to 60% at 10 min, reached 100% at 30 min, and eluted for 10 min (Figure S11). The major peak was collected and subjected to structural analysis.

4.4. Structure Analysis of the Isolated Compound

The chemical structure of the isolated compound was analyzed via mass spectrometry and NMR. The molecular weight was determined to be 358 by ESI-mass measurement, which showed quasi-molecular ion peaks at m/z 359.4 $[\text{M} + \text{H}]^+$ and 381.3 $[\text{M} + \text{Na}]^+$ in positive mode and at m/z 357.3 $[\text{M} - \text{H}]^-$ in negative mode (see Supplementary Material Figure S1). The ^1H NMR spectrum measured in CD_3OD exhibited signals because of 6 aromatic methine protons at δ 7.18 (d, $J = 1.8$ Hz), 7.06 (dd, $J = 8.4, 1.8$ Hz), 6.80 (d, $J = 8.4$ Hz), 6.77 (d, $J = 1.8$ Hz), 6.70 (d, $J = 8.4$ Hz), and 6.63 (dd, $J = 8.4, 1.8$ Hz), which are attributable to 2 1,2,4-trisubstituted benzenes, 2 olefinic methines at δ 7.57 (d, $J = 16.2$ Hz) and 6.35 (d, $J = 16.2$ Hz), which were assigned to a *trans*-1,2-disubstituted double bond, 1 oxygenated methylene at δ 4.16, 2 methylenes at δ 2.65 and 1.97, and 2 methoxy groups at δ 3.89 and 3.82 (see Supplementary Material Figure S2). The ^{13}C NMR spectrum in combination with the HMQC spectrum revealed 20 carbon peaks, including an ester carbonyl carbon at δ 169.4; 4 oxygenated sp^2 carbons at δ 150.8, 149.4, 148.9, and 145.7; 8 sp^2 methine carbons at δ 146.7, 124.1, 121.9, 116.5, 116.2, 115.5, 113.2, and 111.7; 2 sp^2 carbons at δ 134.2 and 127.6; 3 methylene carbons at δ 64.9, 32.8, and 31.8; and 2 methoxy carbons at δ 56.4 and 56.3 (see Supplementary Material Figures S3 and S4). The ^1H - ^1H COSY spectrum established four partial structures, and two 1,2,4-trisubstituted benzenes, $-\text{CH}_2-\text{CH}_2-\text{CH}_2-$, and $-\text{CH}=\text{CH}-$ (see Supplementary Material Figure S5). Further structural elucidation was performed

using the HMBC spectrum, which showed a long-range correlation from the methylene protons at δ 2.65 to the carbons at δ 134.2, 121.9, and 113.2, from the methine proton at δ 7.57 to the carbons at δ 127.6, 124.1, and 111.7, and from the methine protons at δ 7.57 and 6.35 and the methylene protons at δ 4.16 to the carbonyl carbon at δ 169.4. Finally, 2 methoxy protons at δ 3.89 and 3.82 exhibited long-range correlations with the oxygenated sp^2 carbons at δ 149.4 and 148.9, respectively (see Supplementary Materials Figures S6 and S7). Thus, the structure of the isolated compound was identified as dihydroconiferyl ferulate (Figure 2).

4.5. Culture of Human Breast Cancer Cells and Mammospheres

MDA-MA-231 and MCF-7 were purchased from the Korea Cell Line Bank (Seoul, Korea) and cultured in Dulbecco's Modified Eagle's Medium containing 10% fetal bovine serum (Corning, Glendale, AZ, USA) and 1% penicillin/streptomycin solution (Corning) in an incubator with a 5% CO_2 atmosphere. MDA-MA-231 (1×10^4 per well) and MCF-7 (4×10^4 per well) were incubated in a 24- or 6-well ultralow attachment plate with MammoCultTM culture medium (StemCell Technologies, Vancouver, BC, Canada) containing hydrocortisone (0.5 μ g/mL) and heparin (4 μ g/mL) for 7 days.

4.6. Cell Proliferation and Mammosphere Formation Assay

MCF-7 (1.5×10^6 cells/plate) and MDA-MB-231 (1×10^6 cells/plate) cancer cells were seeded into 96-well plates for 24 h and incubated with dihydroconiferyl ferulate (0, 10, 25, 50, 75, 100, 150, and 200 μ M) for 24 h. Subsequently, cell viability was examined using the EZ-Cytox Plus Kit (DoGenBio, Seoul, Korea), according to the manufacturer's protocol. A VERSA_{max} ELISA reader (Molecular Device, San Jose, CA, USA) was used to measure the OD₄₅₀. MDA-MA-231 (1×10^4 per well) and MCF-7 (4×10^4 per well) were incubated in a 6-well ultralow attachment plate with MammoCultTM culture medium for 7 days. Mammospheres were scanned and analyzed using the NIST integrated colony enumerator program [61]. The rate of mammosphere formation was measured by determining the mammosphere formation efficiency (MFE) [62].

4.7. CD44⁺/CD24⁻ Expression and Apoptosis via Flow Cytometry and Mammosphere Growth Assay

MDA-MB-231 cancer cells (1.5×10^6 cells) were cultured in a 6-well plate for 24 h and treated with DMSO as control or dihydroconiferyl ferulate (50 μ M) for 24 h [63]. The cells were harvested, dissociated, and incubated with monoclonal antibody antihuman CD44 (FITC-conjugated) and monoclonal antibody antihuman CD24 (APC-conjugated) antibodies (BD) for 45 min at 4 °C. After washing with 1X PBS, the CD44⁺/CD24⁻ cell populations were examined using an Accuri C6 machine (BD San Jose, CA, USA). The Annexin V Apoptosis Detection kit with PI (BD) was used to measure apoptosis of the mammospheres treated with dihydroconiferyl ferulate (50 μ M) following the manufacturer's protocol. Mammospheres were collected and dissociated with 0.05% trypsin-EDTA 1X (Corning). Briefly, 1×10^6 cells were incubated with Annexin V (FITC) and PI in a binding buffer at room temperature (RT), protected from light for 30 min, and the cells were examined via flow cytometry at the Jeju Center of Korea Basic Science Institute (core facility center, Jeju, South Korea). Mammospheres derived from MDA-MB-231 cells cultured with or without dihydroconiferyl ferulate (50 μ M) were divided into single cells, and an equal number of cancer cells were seeded into six-well plates. The number of cells was counted at 24, 48, and 72 h to measure the growth of the mammospheres.

4.8. Western Blot Analysis

Western blot analysis was conducted on the basis of a previously described method [64]. Protein extracts of mammospheres derived from MDA-MB-231 cells (1×10^4 per well) treated with dihydroconiferyl ferulate (50 μ M) were analyzed using SDS-PAGE (8%) and electrotransferred to polyvinylidene difluoride membranes (Millipore, Billerica, MA, USA).

The membranes were incubated at RT for 1 h in Odyssey blocking buffer (LI-COR, Lincoln, NB, USA) containing Tween 20 (0.1%, *v/v*). The membranes were then incubated overnight at 4 °C in a blocking buffer containing the following primary antibodies: anti-EGFR (#4267s, Cell Signaling Technology, Denver, CO, USA), anti-pStat3 (#9145s, Cell Signaling Technology, Denver, CO, USA), anti-c-Myc (#5605s, Cell Signaling Technology, Denver, CO, USA), anti-Stat3 (sc-482), anti-Lamin B (sc-6216), and anti- β -actin (sc-47778 Santa Cruz Biotechnology, Dallas, TX, USA). The membranes were washed with PBST (phosphate-buffered saline with Tween 20, 0.1%, *v/v*) and incubated with anti-rabbit (IRDye 800CW-conjugated), anti-goat (IRDye 680RD-conjugated), or anti-mouse (IRDye 680RD-conjugated) secondary antibodies. An ODYSSEY CLx machine (LI-COR, Lincoln, NB, USA) was used to examine the band signals.

4.9. Immunoprecipitation (IP)

Proteins extracts of mammospheres treated with DMSO as a control or dihydroconiferyl ferulate (50 μ M) were prepared in lysis buffer (20 mM Hepes, 10 mM EGTA, 40 mM glycerol 2-phosphate, 2.5 mM MgCl₂ 6H₂O, 1% NP-40, pH 7.5). IP was performed using 1 μ g of Stat3 antibody (sc-482) and 500 μ g of protein. Protein A/G-Agarose (P9203-100, GenDEPOT) was used to precipitate the protein complex, which was then analyzed using SDS-PAGE, followed by immunoblotting with the EGFR antibody (#4267s).

4.10. RNA Extraction and qRT-PCR

RNA extraction and qRT-PCR were performed as described previously [64]. Total RNA was isolated from MDA-MB-231 cancer cells or mammospheres using the TaKaRa MiniBEST Universal RNA Extraction Kit according to the manufacturer's protocol. We used the TOPreal™ One-step RT-qPCR kit (SYBR Green with low ROX, Enzygnomics, Daejeon, Korea) for performing qRT-PCR. All gene-specific primers were purchased from Bioneer (Daejeon, Korea). The β -actin gene was used as an internal control (Table S1).

4.11. Stat3 and c-Myc Knockdown Using Small Interfering RNA (siRNA)

MDA-MB-231 cells (1×10^6) were seeded into 6-well plates for 24 h and transfected with human c-Myc-specific siRNAs from Bioneer (Daejeon, Korea) for 48 h to confirm the effect of the c-Myc protein on mammosphere formation and with human Stat3-specific siRNA from Bioneer (Daejeon, Korea) to determine the effect of Stat3 on the expression of the c-Myc protein. We used Lipofectamine 2000 (Invitrogen, Carlsbad, CA, USA) for siRNA transfection of the breast cancer cells. Immunoblotting was performed to examine the expression levels of c-Myc and Stat3 following specific siRNA transfection.

4.12. Statistical Analysis

All data are shown as the mean \pm standard deviation. The differences among the means were analyzed using a one-way ANOVA and a Student's *t*-test; *p* values of <0.05 were considered statistically significant (GraphPad Prism 7 software).

5. Conclusions

Dihydroconiferyl ferulate isolated from *Dendropanax morbiferus* H.Lév. inhibits the proliferation of breast cancer cell lines and mammosphere formation. It reduces the population of CD44^{high}/CD24[−] cells, induces apoptosis, suppresses the proliferation of mammospheres, decreases total and nuclear EGFR, inhibits EGFR/Stat3 complex formation, nuclear Stat3 and pStat3 protein, and subsequently inhibits the transcription and expression of c-Myc. Our results show that dihydroconiferyl ferulate exhibits anti-BCSC activity through the nEGFR/Stat3/c-Myc signaling pathway.

Supplementary Materials: The following supporting information can be downloaded at: <https://www.mdpi.com/article/10.3390/ph15060664/s1>. Figure S1. LC-ESI-mass spectrometry of the purified compound. Figure S2. 1H NMR spectrum of the purified compound. Figure S3. ¹³C

NMR spectrum of the purified compound. Figure S4. HMQC spectrum of the purified compound. Figure S5. ^1H - ^1H COSY spectrum of the purified compound. Figure S6. HMBC spectrum of the purified compound. Figure S7. Two-dimensional NMR correlations and ^1H , ^{13}C peak assignments of the purified compound. Figure S8. The purification procedure of a mammosphere formation inhibitor derived from *Dendropanax morbiferus* H.Lév. using silica gel column chromatography. (A) The sample was isolated by silica gel chromatography with a solvent mixture (CHCl_3 : MeOH (10:1)). (B) TLC plate analysis of the purified sample (CHCl_3 : MeOH = 10:1). Active fraction: #4. Figure S9. The purification procedure of a mammosphere formation inhibitor derived from *Dendropanax morbiferus* H.Lév. using Sephadex LH-20 column chromatography. (A) The sample was isolated by Sephadex LH-20 column chromatography with MeOH. (B) TLC plate analysis of the purified sample (CHCl_3 : MeOH = 10:1). Active fraction: #3. Figure S10. The purification procedure of a mammosphere formation inhibitor derived from *Dendropanax morbiferus* H.Lév. using preparative thin layer chromatography with CHCl_3 :MeOH (10:1). (A) Preparatory TLC chromatography. (B) TLC plate analysis of the prepared TLC bands after the samples were scraped and purified (CHCl_3 :MeOH = 10:1). Figure S11. Purification of a mammosphere formation inhibitor derived from *Dendropanax morbiferus* H.Lév. using HPLC. (A) Assessment of the major fraction using HPLC. Samples were collected based on the 220 nm wavelengths. (B) TLC plate analysis of the purified sample (CHCl_3 :MeOH = 10:1). Figure S12. Purification scheme of a mammosphere formation inhibitor derived from *Dendropanax morbiferus* H.Lév. Table S1. Specific real-time RT-qPCR primer sequences containing Nanog, CD44, Oct4, c-myc, Sox2, and β -actin genes.

Author Contributions: Y.-C.K. and R.L. were responsible for the conceptualization, investigation, formal analysis, and writing. H.-N.S. and B.-S.Y. were responsible for the methodology and formal analysis. H.S.C. and D.-S.L. were responsible for the conceptualization, funding, writing, reviewing, and editing. All authors have read and agreed to the published version of the manuscript.

Funding: This study was supported by the Basic Science Research Program through the National Research Foundation of Korea (NRF) funded by the Ministry of Education (NRF-2016R1A6A1A03012862 and NRF-2020R1A2C1006316). This study was supported by the Korea Basic Science Institute (National Research Facilities and Equipment Center) grant, funded by the Ministry of Education (Grant No. 2020R1A6C101A188). This research was supported by the National University Development Project, funded by the Ministry of Education (Korea) and the National Research Foundation of Korea (2022).

Institutional Review Board Statement: Not applicable.

Informed Consent Statement: Not applicable.

Data Availability Statement: All data is contained within article and supporting information. In addition, the datasets generated in this study are available upon request to the corresponding author.

Conflicts of Interest: All authors declare no conflict of interest.

References

1. Sung, H.; Ferlay, J.; Siegel, R.L.; Laversanne, M.; Soerjomataram, I.; Jemal, A.; Bray, F. Global cancer statistics 2020: GLOBOCAN estimates of incidence and mortality worldwide for 36 cancers in 185 countries. *CA Cancer J. Clin.* **2021**, *71*, 209–249. [[CrossRef](#)] [[PubMed](#)]
2. Loibl, S.; Poortmans, P.; Morrow, M.; Denkert, C.; Curigliano, G. Breast cancer. *Lancet* **2021**, *397*, 1750–1769. [[CrossRef](#)]
3. Harris, L.; Fritsche, H.; Mennel, R.; Norton, L.; Ravdin, P.; Taube, S.; Somerfield, M.R.; Hayes, D.F.; Bast, R.C. American Society of Clinical Oncology 2007 update of recommendations for the use of tumor markers in breast cancer. *J. Clin. Oncol.* **2007**, *25*, 5287–5312. [[CrossRef](#)]
4. Waks, A.G.; Winer, E.P. Breast Cancer Treatment: A Review. *JAMA* **2019**, *321*, 288–300. [[CrossRef](#)] [[PubMed](#)]
5. The Cancer Genome Atlas Network. Comprehensive molecular portraits of human breast tumours. *Nature* **2012**, *490*, 61–70. [[CrossRef](#)] [[PubMed](#)]
6. Collina, F.; Di Bonito, M.; Li Bergolis, V.; De Laurentiis, M.; Vitagliano, C.; Cerrone, M.; Nuzzo, F.; Cantile, M.; Botti, G. Prognostic Value of Cancer Stem Cells Markers in Triple-Negative Breast Cancer. *Biomed. Res. Int.* **2015**, *2015*, 158682. [[CrossRef](#)] [[PubMed](#)]
7. Nusse, R. Wnt signaling and stem cell control. *Cell Res.* **2008**, *18*, 523–527. [[CrossRef](#)]
8. Mavila, N.; Thundimadathil, J. The Emerging Roles of Cancer Stem Cells and Wnt/Beta-Catenin Signaling in Hepatoblastoma. *Cancers* **2019**, *11*, 1406. [[CrossRef](#)]

9. Hsu, E.C.; Kulp, S.K.; Huang, H.L.; Tu, H.J.; Salunke, S.B.; Sullivan, N.J.; Sun, D.; Wicha, M.S.; Shapiro, C.L.; Chen, C.S. Function of Integrin-Linked Kinase in Modulating the Stemness of IL-6-Abundant Breast Cancer Cells by Regulating gamma-Secretase-Mediated Notch1 Activation in Caveolae. *Neoplasia* **2015**, *17*, 497–508. [[CrossRef](#)]
10. Cordenonsi, M.; Zanconato, F.; Azzolin, L.; Forcato, M.; Rosato, A.; Frasson, C.; Inui, M.; Montagner, M.; Parenti, A.R.; Poletti, A.; et al. The Hippo transducer TAZ confers cancer stem cell-related traits on breast cancer cells. *Cell* **2011**, *147*, 759–772. [[CrossRef](#)]
11. Simoes, B.M.; Santiago-Gomez, A.; Chiodo, C.; Moreira, T.; Conole, D.; Lovell, S.; Alferez, D.; Eyre, R.; Spence, K.; Sarmiento-Castro, A.; et al. Targeting STAT3 signaling using stabilised sulforaphane (SFX-01) inhibits endocrine resistant stem-like cells in ER-positive breast cancer. *Oncogene* **2020**, *39*, 4896–4908. [[CrossRef](#)] [[PubMed](#)]
12. Yang, A.; Qin, S.; Schulte, B.A.; Ethier, S.P.; Tew, K.D.; Wang, G.Y. MYC Inhibition Depletes Cancer Stem-like Cells in Triple-Negative Breast Cancer. *Cancer Res.* **2017**, *77*, 6641–6650. [[CrossRef](#)] [[PubMed](#)]
13. Oh, K.; Lee, O.Y.; Park, Y.; Seo, M.W.; Lee, D.S. IL-1beta induces IL-6 production and increases invasiveness and estrogen-independent growth in a TG2-dependent manner in human breast cancer cells. *BMC Cancer* **2016**, *16*, 724. [[CrossRef](#)] [[PubMed](#)]
14. Singh, J.K.; Simoes, B.M.; Howell, S.J.; Farnie, G.; Clarke, R.B. Recent advances reveal IL-8 signaling as a potential key to targeting breast cancer stem cells. *Breast Cancer Res.* **2013**, *15*, 210. [[CrossRef](#)] [[PubMed](#)]
15. Roskoski, R., Jr. The ErbB/HER family of protein-tyrosine kinases and cancer. *Pharmacol. Res.* **2014**, *79*, 34–74. [[CrossRef](#)]
16. Kallergi, G.; Agelaki, S.; Kalykaki, A.; Stournaras, C.; Mavroudis, D.; Georgoulas, V. Phosphorylated EGFR and PI3K/Akt signaling kinases are expressed in circulating tumor cells of breast cancer patients. *Breast Cancer Res.* **2008**, *10*, R80. [[CrossRef](#)]
17. Roberts, P.J.; Der, C.J. Targeting the Raf-MEK-ERK mitogen-activated protein kinase cascade for the treatment of cancer. *Oncogene* **2007**, *26*, 3291–3310. [[CrossRef](#)]
18. Gao, S.P.; Mark, K.G.; Leslie, K.; Pao, W.; Motoi, N.; Gerald, W.L.; Travis, W.D.; Bornmann, W.; Veach, D.; Clarkson, B.; et al. Mutations in the EGFR kinase domain mediate STAT3 activation via IL-6 production in human lung adenocarcinomas. *J. Clin. Investig.* **2007**, *117*, 3846–3856. [[CrossRef](#)]
19. Wee, P.; Wang, Z. Epidermal Growth Factor Receptor Cell Proliferation Signaling Pathways. *Cancers* **2017**, *9*, 52. [[CrossRef](#)]
20. Lin, S.Y.; Makino, K.; Xia, W.; Matin, A.; Wen, Y.; Kwong, K.Y.; Bourguignon, L.; Hung, M.C. Nuclear localization of EGF receptor and its potential new role as a transcription factor. *Nat. Cell Biol.* **2001**, *3*, 802–808. [[CrossRef](#)]
21. Giri, D.K.; Ali-Seyed, M.; Li, L.Y.; Lee, D.F.; Ling, P.; Bartholomeusz, G.; Wang, S.C.; Hung, M.C. Endosomal transport of ErbB-2: Mechanism for nuclear entry of the cell surface receptor. *Mol. Cell Biol.* **2005**, *25*, 11005–11018. [[CrossRef](#)]
22. Lo, H.W.; Hung, M.C. Nuclear EGFR signalling network in cancers: Linking EGFR pathway to cell cycle progression, nitric oxide pathway and patient survival. *Br. J. Cancer* **2006**, *94*, 184–188. [[CrossRef](#)] [[PubMed](#)]
23. Shi, Y.; Liu, N.; Lai, W.; Yan, B.; Chen, L.; Liu, S.; Liu, S.; Wang, X.; Xiao, D.; Liu, X.; et al. Nuclear EGFR-PKM2 axis induces cancer stem cell-like characteristics in irradiation-resistant cells. *Cancer Lett.* **2018**, *422*, 81–93. [[CrossRef](#)] [[PubMed](#)]
24. Kim, J.H.; Choi, H.S.; Lee, D.S. Primaquine Inhibits the Endosomal Trafficking and Nuclear Localization of EGFR and Induces the Apoptosis of Breast Cancer Cells by Nuclear EGFR/Stat3-Mediated c-Myc Downregulation. *Int. J. Mol. Sci.* **2021**, *22*, 12961. [[CrossRef](#)] [[PubMed](#)]
25. Balakrishnan, R.; Cho, D.Y.; Su-Kim, I.; Choi, D.K. *Dendropanax Morbiferus* and Other Species from the Genus *Dendropanax*: Therapeutic Potential of Its Traditional Uses, Phytochemistry, and Pharmacology. *Antioxidants* **2020**, *9*, 962. [[CrossRef](#)]
26. Hyun, T.K.; Kim, M.O.; Lee, H.; Kim, Y.; Kim, E.; Kim, J.S. Evaluation of anti-oxidant and anti-cancer properties of *Dendropanax morbifera* Leveille. *Food Chem.* **2013**, *141*, 1947–1955. [[CrossRef](#)]
27. Chung, I.M.; Song, H.K.; Kim, S.J.; Moon, H.I. Anticomplement activity of polyacetylenes from leaves of *Dendropanax morbifera* Leveille. *Phytother. Res.* **2011**, *25*, 784–786. [[CrossRef](#)]
28. Moon, H.I. Antidiabetic effects of dendropanoxide from leaves of *Dendropanax morbifera* Leveille in normal and streptozotocin-induced diabetic rats. *Hum. Exp. Toxicol.* **2011**, *30*, 870–875. [[CrossRef](#)]
29. Kim, W.; Kim, D.W.; Yoo, D.Y.; Jung, H.Y.; Kim, J.W.; Kim, D.W.; Choi, J.H.; Moon, S.M.; Yoon, Y.S.; Hwang, I.K. Antioxidant effects of *Dendropanax morbifera* Leveille extract in the hippocampus of mercury-exposed rats. *BMC Complement Altern. Med.* **2015**, *15*, 247. [[CrossRef](#)]
30. Brand, T.M.; Iida, M.; Luthar, N.; Starr, M.M.; Huppert, E.J.; Wheeler, D.L. Nuclear EGFR as a molecular target in cancer. *Radiother. Oncol.* **2013**, *108*, 370–377. [[CrossRef](#)]
31. Lo, H.W.; Hsu, S.C.; Ali-Seyed, M.; Gunduz, M.; Xia, W.; Wei, Y.; Bartholomeusz, G.; Shih, J.Y.; Hung, M.C. Nuclear interaction of EGFR and STAT3 in the activation of the iNOS/NO pathway. *Cancer Cell* **2005**, *7*, 575–589. [[CrossRef](#)] [[PubMed](#)]
32. Bhat, A.A.; Lu, H.; Soutto, M.; Capobianco, A.; Rai, P.; Zaika, A.; El-Rifai, W. Exposure of Barrett's and esophageal adenocarcinoma cells to bile acids activates EGFR-STAT3 signaling axis via induction of APE1. *Oncogene* **2018**, *37*, 6011–6024. [[CrossRef](#)] [[PubMed](#)]
33. Harada, D.; Takigawa, N.; Kiura, K. The Role of STAT3 in Non-Small Cell Lung Cancer. *Cancers* **2014**, *6*, 708–722. [[CrossRef](#)] [[PubMed](#)]
34. Kim, R.W.; Lee, S.Y.; Kim, S.G.; Heo, Y.R.; Son, M.K. Antimicrobial, Antioxidant and Cytotoxic Activities of *Dendropanax morbifera* Leveille extract for mouthwash and denture cleaning solution. *J. Adv. Prosthodont.* **2016**, *8*, 172–180. [[CrossRef](#)] [[PubMed](#)]
35. Yun, J.W.; Kim, S.H.; Kim, Y.S.; Choi, E.J.; You, J.R.; Cho, E.Y.; Yoon, J.H.; Kwon, E.; Kim, H.C.; Jang, J.J.; et al. Preclinical study of safety of *Dendropanax morbifera* Leveille leaf extract: General and genetic toxicology. *J. Ethnopharmacol.* **2019**, *238*, 111874. [[CrossRef](#)]

36. Wang, C.; Mathiyalagan, R.; Kim, Y.J.; Castro-Aceituno, V.; Singh, P.; Ahn, S.; Wang, D.; Yang, D.C. Rapid green synthesis of silver and gold nanoparticles using *Dendropanax morbifera* leaf extract and their anticancer activities. *Int. J. Nanomed.* **2016**, *11*, 3691–3701.
37. Sachan, R.; Kundu, A.; Dey, P.; Son, J.Y.; Kim, K.S.; Lee, D.E.; Kim, H.R.; Park, J.H.; Lee, S.H.; Kim, J.H.; et al. *Dendropanax morbifera* Protects against Renal Fibrosis in Streptozotocin-Induced Diabetic Rats. *Antioxidants* **2020**, *9*, 84. [[CrossRef](#)]
38. Choi, J.H.; Kim, S. Antioxidant and antithrombotic properties of *Dendropanax morbifera* Leveille (Araliaceae) and its ferments produced by fermentation processing. *J. Food Biochem.* **2019**, *43*, e13056. [[CrossRef](#)]
39. Youn, J.S.; Kim, Y.J.; Na, H.J.; Jung, H.R.; Song, C.K.; Kang, S.Y.; Kim, J.Y. Antioxidant activity and contents of leaf extracts obtained from *Dendropanax morbifera* LEV are dependent on the collecting season and extraction conditions. *Food Sci. Biotechnol.* **2019**, *28*, 201–207. [[CrossRef](#)]
40. Akram, M.; Kim, K.A.; Kim, E.S.; Syed, A.S.; Kim, C.Y.; Lee, J.S.; Bae, O.N. Potent Anti-inflammatory and Analgesic Actions of the Chloroform Extract of *Dendropanax morbifera* Mediated by the Nrf2/HO-1 Pathway. *Biol. Pharm. Bull.* **2016**, *7*, 728–736. [[CrossRef](#)]
41. Birhanu, B.T.; Kim, J.Y.; Hossain, M.A.; Choi, J.W.; Lee, S.P.; Park, S.C. An in vivo immunomodulatory and anti-inflammatory study of fermented *Dendropanax morbifera* Leveille leaf extract. *BMC Complement Altern. Med.* **2018**, *18*, 222. [[CrossRef](#)] [[PubMed](#)]
42. Eom, T.; Ko, G.; Kim, K.C.; Kim, J.S.; Unno, T. *Dendropanax morbifera* Leaf Extracts Improved Alcohol Liver Injury in Association with Changes in the Gut Microbiota of Rats. *Antioxidants* **2020**, *9*, 911. [[CrossRef](#)] [[PubMed](#)]
43. Park, S.Y.; Karthivashan, G.; Ko, H.M.; Cho, D.Y.; Kim, J.; Cho, D.J.; Ganesan, P.; Su-Kim, I.; Choi, D.K. Aqueous Extract of *Dendropanax morbiferus* Leaves Effectively Alleviated Neuroinflammation and Behavioral Impediments in MPTP-Induced Parkinson's Mouse Model. *Oxid. Med. Cell Longev.* **2018**, *2018*, 3175214. [[CrossRef](#)] [[PubMed](#)]
44. Yoo, D.Y.; Jung, H.Y.; Kwon, H.J.; Kim, J.W.; Nam, S.M.; Chung, J.Y.; Choi, J.H.; Kim, D.W.; Yoon, Y.S.; Hwang, I.K. Effects of *Dendropanax morbifera* Leveille extract on hypothyroidism-induced oxidative stress in the rat hippocampus. *Food Sci. Biotechnol.* **2016**, *25*, 1761–1766. [[CrossRef](#)]
45. Lee, J.W.; Kim, K.S.; An, H.K.; Kim, C.H.; Moon, H.I.; Lee, Y.C. *Dendropanoxide* induces autophagy through ERK1/2 activation in MG-63 human osteosarcoma cells and autophagy inhibition enhances *dendropanoxide*-induced apoptosis. *PLoS ONE* **2013**, *8*, e83611. [[CrossRef](#)]
46. Lee, S.H.; Seo, G.S.; Kim, H.S.; Woo, S.W.; Ko, G.; Sohn, D.H. 2',4',6'-Tris(methoxymethoxy) chalcone attenuates hepatic stellate cell proliferation by a heme oxygenase-dependent pathway. *Biochem. Pharmacol.* **2006**, *72*, 1322–1333. [[CrossRef](#)]
47. Cho, S.G.; Woo, S.M.; Ko, S.G. Butein suppresses breast cancer growth by reducing a production of intracellular reactive oxygen species. *J. Exp. Clin. Cancer Res.* **2014**, *33*, 51. [[CrossRef](#)]
48. Yit, C.C.; Das, N.P. Cytotoxic effect of butein on human colon adenocarcinoma cell proliferation. *Cancer Lett.* **1994**, *82*, 65–72. [[CrossRef](#)]
49. Hsu, Y.K.; Chen, H.Y.; Wu, C.C.; Huang, Y.C.; Hsieh, C.P.; Su, P.F.; Huang, Y.F. Butein induces cellular senescence through reactive oxygen species-mediated p53 activation in osteosarcoma U-2 OS cells. *Environ. Toxicol.* **2021**, *36*, 773–781. [[CrossRef](#)]
50. Ishikawa, C.; Senba, M.; Mori, N. Butein inhibits NF-kappaB, AP-1 and Akt activation in adult T-cell leukemia/lymphoma. *Int. J. Oncol.* **2017**, *51*, 633–643. [[CrossRef](#)]
51. Pandey, M.K.; Sung, B.; Ahn, K.S.; Aggarwal, B.B. Butein suppresses constitutive and inducible signal transducer and activator of transcription (STAT) 3 activation and STAT3-regulated gene products through the induction of a protein tyrosine phosphatase SHP-1. *Mol. Pharmacol.* **2009**, *75*, 525–533. [[CrossRef](#)] [[PubMed](#)]
52. Yang, E.B.; Guo, Y.J.; Zhang, K.; Chen, Y.Z.; Mack, P. Inhibition of epidermal growth factor receptor tyrosine kinase by chalcone derivatives. *Biochim. Biophys. Acta.* **2001**, *1550*, 144–152. [[CrossRef](#)]
53. Jung, S.K.; Lee, M.H.; Lim, D.Y.; Lee, S.Y.; Jeong, C.H.; Kim, J.E.; Lim, T.G.; Chen, H.; Bode, A.M.; Lee, H.J.; et al. Butein, a novel dual inhibitor of MET and EGFR, overcomes gefitinib-resistant lung cancer growth. *Mol. Carcinog.* **2015**, *54*, 322–331. [[CrossRef](#)] [[PubMed](#)]
54. Giordano, A.; Tommonaro, G. Curcumin and Cancer. *Nutrients* **2019**, *11*, 2376. [[CrossRef](#)] [[PubMed](#)]
55. Lee, J.Y.; Lee, Y.M.; Chang, G.C.; Yu, S.L.; Hsieh, W.Y.; Chen, J.J.; Chen, H.W.; Yang, P.C. Curcumin induces EGFR degradation in lung adenocarcinoma and modulates p38 activation in intestine: The versatile adjuvant for gefitinib therapy. *PLoS ONE* **2011**, *6*, e23756. [[CrossRef](#)]
56. Eldredge, E.R.; Korf, G.M.; Christensen, T.A.; Connolly, D.C.; Getz, M.J.; Maihle, N.J. Activation of c-fos gene expression by a kinase-deficient epidermal growth factor receptor. *Mol. Cell Biol.* **1994**, *14*, 7527–7534.
57. Lo, H.W.; Cao, X.; Zhu, H.; Ali-Osman, F. Cyclooxygenase-2 is a novel transcriptional target of the nuclear EGFR-STAT3 and EGFRvIII-STAT3 signaling axes. *Mol. Cancer Res.* **2010**, *8*, 232–245. [[CrossRef](#)]
58. Hung, L.Y.; Tseng, J.T.; Lee, Y.C.; Xia, W.; Wang, Y.N.; Wu, M.L.; Chuang, Y.H.; Lai, C.H.; Chang, W.C. Nuclear epidermal growth factor receptor (EGFR) interacts with signal transducer and activator of transcription 5 (STAT5) in activating Aurora-A gene expression. *Nucleic Acids Res.* **2008**, *36*, 4337–4351. [[CrossRef](#)]
59. Shien, K.; Toyooka, S.; Yamamoto, H.; Soh, J.; Jida, M.; Thu, K.L.; Hashida, S.; Maki, Y.; Ichihara, E.; Asano, H.; et al. Acquired resistance to EGFR inhibitors is associated with a manifestation of stem cell-like properties in cancer cells. *Cancer Res.* **2013**, *73*, 3051–3061. [[CrossRef](#)]

60. Liu, R.; Choi, H.S.; Kim, S.L.; Kim, J.H.; Yun, B.S.; Lee, D.S. 6-Methoxymellein Isolated from Carrot (*Daucus carota* L.) Targets Breast Cancer Stem Cells by Regulating NF-kappaB Signaling. *Molecules* **2020**, *25*, 4374. [[CrossRef](#)]
61. Clarke, M.L.; Burton, R.L.; Hill, A.N.; Litorja, M.; Nahm, M.H.; Hwang, J. Low-cost, high-throughput, automated counting of bacterial colonies. *Cytometry A* **2010**, *77*, 790–797. [[CrossRef](#)] [[PubMed](#)]
62. Choi, H.S.; Kim, D.A.; Chung, H.; Park, I.H.; Kim, B.H.; Oh, E.S.; Kang, D.H. Screening of breast cancer stem cell inhibitors using a protein kinase inhibitor library. *Cancer Cell Int.* **2017**, *17*, 25. [[CrossRef](#)] [[PubMed](#)]
63. Zhen, X.; Choi, H.S.; Kim, J.H.; Kim, S.L.; Liu, R.; Yun, B.S.; Lee, D.S. Machilin D, a Lignin Derived from *Saururus chinensis*, Suppresses Breast Cancer Stem Cells and Inhibits NF-kappaB Signaling. *Biomolecules* **2020**, *10*, 245. [[CrossRef](#)] [[PubMed](#)]
64. Choi, H.S.; Kim, S.L.; Kim, J.H.; Deng, H.Y.; Yun, B.S.; Lee, D.S. Triterpene Acid (3-O-p-Coumaroyltormentic Acid) Isolated from Aronia Extracts Inhibits Breast Cancer Stem Cell Formation through Downregulation of c-Myc Protein. *Int. J. Mol. Sci.* **2018**, *19*, 2528. [[CrossRef](#)] [[PubMed](#)]